coatings

MDPI

*Article*

# Mechanical and Spectrophotometric Properties of Nano-$WS_2$ Modified PVB/Epoxy Coatings on Glass

**Danica M. Bajić [1,*], Aleksandra Samolov [2], Bojana Fidanovski [1], Miloš Pavić [1] and Ana Alil [3]**

[1] Military Technical Institute, Ratka Resanovića 1, 11030 Belgrade, Serbia; bojana.fidanovski@mod.gov.rs (B.F.); meelos.pavic@gmail.com (M.P.)
[2] "Vinča" Institute of Nuclear Sciences, National Institute of Republic of Serbia, University of Belgrade, 11351 Belgrade, Serbia; aleksandra.samolov@vin.bg.ac.rs
[3] University of Belgrade, Institute of Chemistry, Technology and Metallurgy, National Institute of the Republic of Serbia, 11000 Belgrade, Serbia; ana.alil@ihtm.bg.ac.rs
* Correspondence: danica.bajic@mod.gov.rs

## Highlights

- Hybrid PVB/epoxy coatings reinforced with $WS_2$ nanostructures (IF + INT);
- Application on glass and as bulk polymer;
- Combined optical + thermo-mechanical + camouflage examination;
- Potential applications in defense technology.

## Abstract

The development of transparent multifunctional coatings capable of combining optical properties with mechanical durability remains a significant challenge in advanced materials engineering. In this study, novel hybrid coatings based on a poly(vinyl butyral)/epoxy resin (PVB/epoxy) matrix reinforced with tungsten disulfide ($WS_2$) nanostructures were developed and examined for potential application in camouflage protection of glass surfaces. Camouflage aims to reduce the detectability of an object by minimizing the optical contrast between the object and its surrounding environment. For transparent substrates such as glass, this objective is particularly demanding because the transparency must be preserved while reducing unwanted surface reflection and optical signatures over relevant spectral ranges. For this purpose, in this research two types of nanostructures were investigated: fullerene-like nanoparticles (IF-$WS_2$) and inorganic nanotubes (INT-$WS_2$). The coatings were fabricated via ultrasonically assisted solution dispersion followed by casting over the glass plates and Teflon molds, and solvent evaporation. Structural, thermal, optical, and mechanical properties were systematically evaluated using SEM, FTIR, DSC, UV-Vis-NIR spectroscopy, gloss measurements, hardness testing, and cavitation wear resistance analysis. The incorporation of $WS_2$ nanostructures led to improved mechanical performance, with increased hardness and enhanced resistance to cavitation-induced wear. Optical characterization showed moderate reductions in reflectance and controlled transmittance in the visible and near-infrared regions, while overall transparency was maintained. The results indicate that $WS_2$ nanostructures contribute to both light scattering and absorption, leading to reduced specular reflection and improved optical masking potential. The findings demonstrate that hybrid PVB/epoxy/$WS_2$ coatings offer a promising approach for designing transparent, mechanically resistant coatings with tunable optical properties, with potential applications in protective glass systems and advanced functional surfaces.



Academic Editor: Gianfranco Carotenuto

Received: 14 June 2026
Revised: 12 July 2026
Accepted: 14 July 2026
Published: 16 July 2026

**Keywords:** coatings on glass; poly(vinyl butyral); epoxy resin; tungsten disulfide; hybrid nanocomposite; spectrophotometric properties

## 1. Introduction

The development of advanced coatings for glass surfaces has been directed towards both functional and protective applications. Among these, coatings that combine desirable mechanical resistance with effective optical properties are of particular interest for aerospace and defense purposes, for anti-reflective or anti-glare applications, as well as for potential camouflage protection. In military applications the term camouflage is used for various means for deceiving an observer, whether it is a person or a specific device making the object of interest less visible. This can be done using different color patterns which can be originally designed or created to look like some object found in nature [1,2].

Radar-absorbent coatings, or stealth coatings, have shown potential for reduced spectral signature and improved optical masking of military aircraft, ships, vehicles and military textile garments, making them less detectable [1,3]. Special thermally controlled coatings for spacecrafts have been developed for applications in the extreme environment of space, since thermal control is critical for protecting spacecraft and maintaining equipment functionality, regulating heat absorption and emission by reflecting or absorbing specific light wavelengths [4,5]. Optical coatings are indispensable in defense applications, from combat aircraft and vehicles to night vision devices, in stealth and camouflage technologies. These coatings also limit infrared detection, improving survivability and mission effectiveness in hostile environments.

In the production of displays there are also commercially available, anti-reflective and anti-glare glass solutions and thin coatings such as inorganic film on *Corning*® *Gorilla*® *Glass*, where surface reflection was reduced by up to 75% to 95%, reducing the glass's signature and improving scratch resistance [6,7]. The thin film on the glass interacts with the incoming light, causing light waves to interfere with each other and reducing the intensity and magnitude of reflected light. In addition to the altered reflectance and absorbance, these functional coatings should be clear and transparent. However, the anti-reflective properties are not important only in the display industry, but also in protection of military vehicles, aircraft, and objects with glass surfaces. There are few available options to provide effective and still transparent camouflage protection of the specified objects, since it is not easy to create wavelength-selective hard coatings with high hardness and mechanical durability, especially when they are not thin ceramic layers [8–10]. Still, in addition to the thin inorganic coatings, there are also some polymer-based and nanomodified coatings for the named applications, like epoxide-silica layers or similar polymer-ceramic coatings [11–16]. It is still challenging to achieve a combination of transparency, wavelength-selective absorption, and mechanical resistance at the same time. Inorganic coatings are often brittle and have processing limitations, and the polymer-based systems typically lack sufficient mechanical resistance or controlled optical functionality.

This research offers a possible solution for this problem, with the development of specially designed hybrid coatings consisting of a clear, transparent polymer matrix based on poly(vinyl butyral), PVB, and epoxy resin, with the addition of functional nanostructures of tungsten disulfide. PVB and epoxy resin are widely recognized for their good adhesion to many surfaces and good miscibility with various fillers and solvents, as well as for their mutual compatibility [17–19]. Epoxy resin is widely used in structural composites due to its mechanical properties, but has also found application in shielding materials and composites for electromagnetic wave absorption [20,21]. Additionally, PVB was widely studied as

a proper polymer matrix for composites of various applications, solely or blended with other polymers [22–28]. This makes the two polymers good candidates for the proposed hybrid coatings. In this study, we introduce a novel composite coating system based on the two selected polymers, reinforced with tungsten disulfide nanostructures: fullerene-like nanoparticles, IF-$WS_2$, and inorganic multi-wall nanotubes, INT-$WS_2$. The reasons for choosing $WS_2$ nanostructures lie in their specific intrinsic properties. The unique morphology of $WS_2$ nanostructures enables dual functionality: fullerene-like nanoparticles are expected to provide isotropic reinforcement and defect mitigation in the material in which they are incorporated, while nanotubes are expected to provide improved load transfer and crack-bridging mechanisms [28–38]. In addition to mechanical reinforcement, the incorporation of $WS_2$ nanostructures in a material/polymer matrix or a coating may provide improved thermal stability as well [39–42], and tuned optical and electromagnetic properties, applicable in shielding technologies [43–47]. Tungsten disulfide is a semiconductor with strong light absorption in the visible and near-infrared (NIR) spectrum. It was reported that $WS_2$ nanosheets show good absorption of electromagnetic waves, due to their graphene-like structure. $WS_2$ structures can absorb 5%–10% of incident sunlight, having a direct band gap of 1.98 eV for the monolayer $WS_2$, and the value of an indirect band gap of 1.3 eV for the multilayer $WS_2$ [43–47].

In the present study, these nanostructures were incorporated into a PVB/epoxy matrix and applied to glass plates, and the resulting coatings were evaluated for their optical and mechanical properties, focusing on their ability to improve camouflage masking, and to enhance the mechanical resistance of the surfaces. By systematically analyzing the impact of $WS_2$ nanostructures on the observed characteristics of the coatings, this research has the aim to provide some new insights into the design of multifunctional glass coatings with promising applications in camouflage technologies. The nanostructures can absorb specific wavelengths, decreasing reflectance and transmittance while contributing to the coating's camouflage by reducing its spectral signature. Research conducted on coatings with $WS_2$ applied on camouflage textile materials showed that the tungsten disulfide's absorption in the near-infrared range reduces the visibility of the coated surface under NIR imaging systems, which are commonly used for detection in camouflage applications. Also, $WS_2$ nanoparticles may reduce the radar cross-section due to their ability to interfere with electromagnetic waves [3,48]. Relying on the inherent properties of fullerene-like nanoparticles and inorganic nanotubes of tungsten disulfide used as reinforcement, multiple improvements in the performance of PVB/epoxy coatings on glass can be expected, such as increased hardness and scratch resistance, i.e., wear resistance of the new material. Also, their addition will alter the coating's optical properties, i.e., affect the camouflage and masking properties, since each individual nanoparticle and nanotube can scatter light and affect specular reflectance (shine), i.e., they will alter the coating's glare and visibility [44,47,48]. While $WS_2$ nanostructures were earlier investigated as incorporated into thin flexible PVB coatings applied on textile substrates for the improvement of their camouflage properties [48], the present work focuses on transparent hybrid coatings PVB/epoxy deposited on rigid glass substrates and investigates the combined effects of $WS_2$ nanostructures on both optical and mechanical performance. It is also important to note that in this study there is a significant amount of epoxy relative to the PVB, so the spectrophotometric properties might be challenging. The proposed new composite coatings with fullerene-like and tubular nanostructures of $WS_2$ in a transparent PVB/epoxy hybrid matrix on glass are targeting simultaneous optical modulation and mechanical reinforcement.

## 2. Materials and Experimental Methods

### *2.1. Preparation of PVB/Epoxy Coatings*

In the phase of the preparation of PVB/epoxy coatings, the following materials and chemicals were used:

- PVB powder Mowital B60H, Kuraray;
- A clear two-component epoxy system, aero-grade epoxy resin system L385 + L386, Hexion;
- Ethanol 96%, Reachem;
- IF-$WS_2$ of declared diameter 40–100 nm, NanoLub, ApNano;
- INT-$WS_2$ (multi-wall) of declared diameter 80–100 nm and length 10–20 μm, NanoLub, ApNano.

The ratio between the epoxy and PVB component in the coatings was 95:5. The selected nanostructures of $WS_2$ were added in the following concentrations: 1.0 wt.% IF-$WS_2$ and 0.3 wt.% INT-$WS_2$. The selected concentrations were chosen based on available literature data and preliminary formulation studies, which indicated that these loadings provide homogeneous dispersion while preserving coating transparency and processability [27,28,33,34,49,50], since the aim of the present work was not to optimize the nanofiller loading, but rather to investigate the influence of two different $WS_2$ nanostructure morphologies (IF-$WS_2$ and INT-$WS_2$) on the structural characteristics, spectrophotometric properties and mechanical resistance of the surface of transparent PVB/epoxy coatings.

In order to successfully design the proposed coatings, several challenges should have been addressed in their manufacturing process. First, knowing the tendency of the selected nanostructures to agglomerate, the method ought to have been found to achieve uniform dispersion of $WS_2$ nanostructures in PVB [33,49,50]. Also, the viscosity of the epoxy components and PVB polymer was a possible obstacle to this uniform dispersion, so a temporary solvent was introduced, which served at the same time as a surface functionalization of $WS_2$ nanostructures, to improve their interfacial adhesion and ensure compatibility with PVB and prevent phase separation.

The first step in the preparation of the hybrid nanocomposite coatings—ultrasonication—was necessary to prevent agglomeration of the nanostructures in the composite. This step was done as a preparation of the particles for the incorporation into the polymer matrix, and the ethanol was used as a solvent. This was performed using an ultrasonic homogenizer Bandelin Sonopuls HD 4100 (BANDELIN electronic GmbH & Co. KG, Berlin, Germany). The device has a 13 mm sonotrode TS 113 made of the titanium alloy $TiAl_6V_4$, with a maximum amplitude of 82 μm. The ultrasonication lasted for 30 min, at 60 W, 20 kHz, and in the continuous mode.

The second step was mixing the particles' dispersion with the polymers (PVB and epoxy): this dispersion was mixed with epoxy L385, then PVB was added in small portions and dissolved in this mixture while still mixing on a mechanical stirrer, and finally epoxy hardener L386 was added.

The third step was the casting of the obtained mixture (polymer solution with the incorporated particles) onto the glass plates, as well as in a flat rectangular Teflon mold to have film-like samples of the coatings. Prior to casting, the glass plate surfaces and the Teflon molds were cleaned first with acetone, then with ethanol and dried.

The last step was solvent evaporation overnight, leaving the solid polymer reinforced with the dispersed particles in it. After the drying at room temperature, the samples were placed in a vacuum drying oven at 60 °C for 6 h, to ensure evaporation of remaining solvent.

In an analogous way, a neat PVB/epoxy coating was prepared, without $WS_2$ nanostructures, as a reference sample. Figure 1 depicts selected phases of the coatings' preparation and the appearance of the prepared coatings on glass plates.

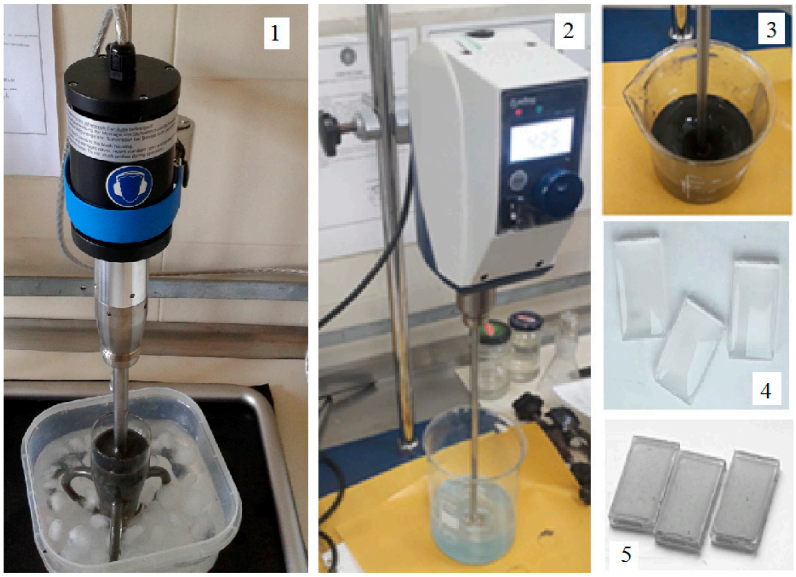


**Figure 1.** Preparation of the PVB/epoxy coatings: (**1**) ultrasonication of IF-$WS_2$ in ethanol, (**2**) PVB/epoxy homogenization, (**3**) PVB/epoxy homogenization with ultrasonicated IF-$WS_2$ in ethanol, (**4**) prepared neat PVB/epoxy coating cast onto the glass plates, (**5**) epoxy/PVB/INT-$WS_2$ coating cast onto the glass plates.

The thickness of the coatings was determined by measuring the glass plates before and after applying the composite coating and after its drying. This measurement was done 3 times per sample, using a digital caliper with an accuracy of ±0.01 mm. Obtained coatings on glass were ~90–110-microns thick. Regarding the samples obtained in the Teflon mold, they were intentionally made thicker: ~1.20–1.35 mm, in order to have proper samples for cavitation wear resistance testing.

### *2.2. Characterization Techniques*

Scanning electron microscopy (SEM) was used to examine the morphology of the nanostructures of $WS_2$ before their incorporation into the PVB/epoxy system, as well as afterwards, to examine the quality of their dispersion in the polymer matrix. The JEOL JSM-6610 LV (JEOL Ltd. Akishima, Tokyo, Japan) device was used for this characterization method.

Particle size analysis was performed using the PSA 1190 Anton Paar device (Graz, Austria) to determine their particle size distribution, in liquid mode, with ethanol as the dispersion medium. The same solvent was selected for this analysis as the solvent used for coating preparation, in order to obtain results as realistic as possible, that is, to determine the particle size distribution as close as possible to that in the coating mixture.

Fourier transform infrared spectroscopy (FTIR) analysis was carried out to examine possible interfacial interactions and structural compatibility between the incorporated nanostructures of tungsten disulfide and the two combined polymers. The Nicolet iS TM 10 spectrometer device was used (Thermo Fisher Scientific, Waltham, MA, USA), with the Attenuated Total Reflectance (ATR) sampling technique.

Differential scanning calorimetry (DSC) analysis was carried out to determine the glass transition temperatures ($T_g$) of the prepared PVB/epoxy coatings, with and without tungsten disulfide. The DSC Q20 device was used (TA Instruments), with Universal V4.7A

data acquisition program. These analyses were carried out in a nitrogen flow (50 ml $min^{-1}$). The samples were first heated from 0 °C to 200 °C at a rate of 10 °C $min^{-1}$, then cooled at the same rate and heated again, within the same temperature range, to obtain a hysteresis curve. These two cycles of heating were necessary to obtain a relevant $T_g$ value, since the first heating scan in DSC provides the removal of residual solvents and releases any remaining thermal stress from the polymer material, and more reproducible values are obtained from the second heating cycle [51].

The hardness was measured in the Shore D scale for plastics, using a manual Zorn Stendall DDR device. For each composite coating, measurements were performed at five different spots on the surface. These measurements were performed at room temperature (approximately 20–24 °C).

Resistance of the polymer composite coatings, in the form of thick film-like samples, to ultrasonic cavitation wear was examined using the above-described processor Bandelin Sonopuls HD 4100. The test was done according to the ultrasonic vibration method with a stationary sample, ASTM G32 standard [52,53]. Although the standard ASTM G32 was originally developed for metallic materials, it has also been successfully applied in examinations of other types of materials [53–55]. In this work it was employed as a comparative method, to evaluate the cavitation erosion resistance of the nanoreinforced formulations in comparison with the referent neat coating PVB/epoxy, i.e., to estimate the beneficial effect of the different morphologies of the used tungsten disulfide reinforcement. The square-shaped specimens for this test were cut from the composite coating samples taken from the Teflon molds, and placed in a vessel with distilled water, fixed to the specimen holder at the bottom of the vessel, 0.5 mm below the ultrasonic probe tip. The samples underwent ultrasonic cavitation in 5 cycles of 15 min, at room temperature (~20 °C). The parameters of the ultrasonic processor were set at the frequency of 20 kHz, and power of 50 W. An ice bath was used to reduce the heating of the system. After each cavitation cycle, the samples were dried to a constant mass, and the weight loss was recorded.

Camouflage properties of the coatings on glass plates were examined by analyzing diffuse reflection, transmittance and specular gloss. The UV/VIS/NIR spectrophotometer Shimadzu UV 3600 device was used to determine both diffuse reflection and transmittance in the VIS and NIR area of the EMS (400–1600 nm), with the UV Probe program package. Samples were placed horizontally in the sample compartment of the device, which has a 2 cm aperture diameter. The measurements were performed according to ASTM E903-12 standard where placement of samples was defined for both types of measurements [56]. Every sample was measured only once. Specular gloss was measured with the Elcometer 480 model T device, at an angle of 20°, which is a standard measurement angle for glazed materials, with measurement uncertainty ±0.2. Measurements were performed five times and the presented values are the mean measurement values. Data management software ElcoMaster V 2.0.61 was used for data acquisition and analysis. The specular gloss values were obtained in accordance with the SRPS EN ISO 2813 standard [57].

## 3. Results and Discussion

### *3.1. SEM/EDS Results*

Figure 2 shows the appearance of the nanostructures and the coatings with the incorporated nanostructures. As observed, the nanostructures initially exhibit some aggregation (Figure 2, panels 1 and 2), but the ultrasonic treatment before their incorporation into the polymer matrix enables their deagglomeration and ensures good distribution throughout the matrix (Figure 2, panels 3 and 4). The ultrasonication provided successful deagglomeration of both fullerene-like nanoparticles and the nanotubes.

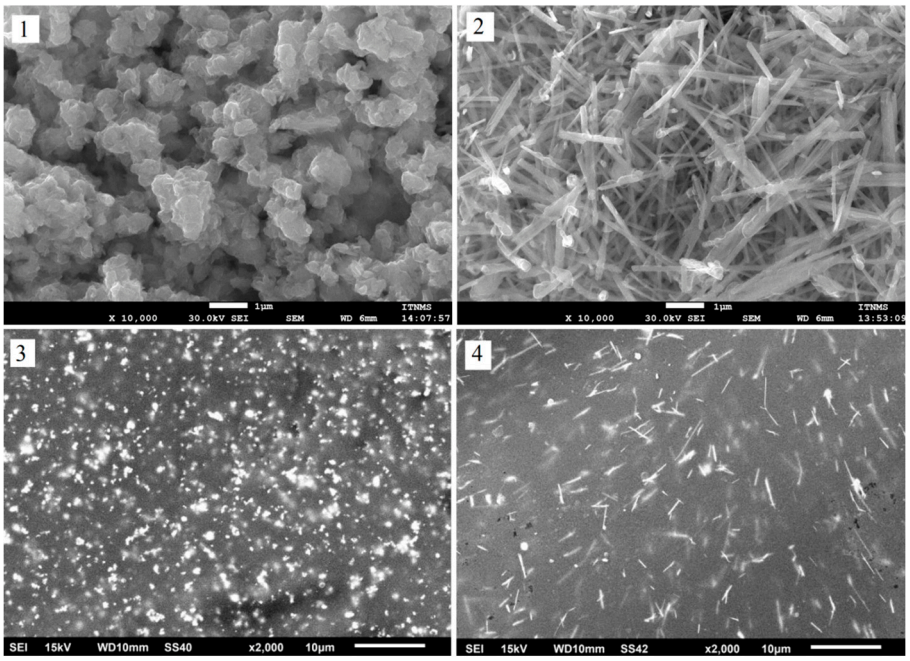


**Figure 2.** SEM images of: (**1**) IF-$WS_2$; (**2**) INT-$WS_2$; (**3**) PVB/epoxy/ IF-$WS_2$; (**4**) PVB/epoxy/ INT-$WS_2$.

### *3.2. PSA Results*

The average particle size and the particle size distribution of IF-$WS_2$ nanoparticles by volume, with the characteristic values of D10, D50 and D90 by volume and by number, are given in Figure 3. The value D10 represents the particle diameter below which 10% of the particle population is found, D50 is the particle diameter below which 50% of the particle population is detected, while D90 corresponds to 90% of the cumulative distribution. There is a difference between volume-based and number-based particle size distributions: the first representation shows the total particle volume in each size class, and the other shows the number of particles in each size class.

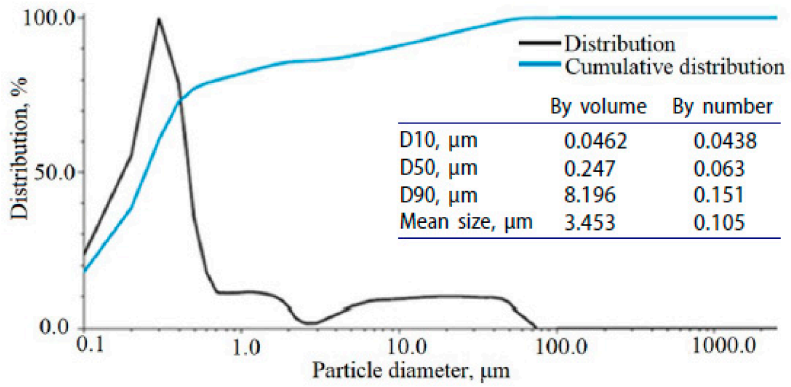


**Figure 3.** Particle size distribution of IF-$WS_2$.

From the observed results, it is evident that the majority of the particles are nanosized although there still remained some micron-sized agglomerates. The graph was cut off at 40 nm, since the device used for PSA cannot measure below this limit of the measuring range. Certainly, there is some quantity of particles smaller than 40 nm, so the obtained D10, D50 and D90 values should be taken with a reserve. This analysis is not applicable to tubular nanostructures, so the average dimensions of INT-$WS_2$ were estimated from SEM images: it was observed that the nanotubes vary in diameter from 70 to 180 nm,

and in length from 5 to 25 microns, but the percentage of different sizes distribution was not determined.

### *3.3. FTIR Results*

The registered FTIR spectra for the examined coatings are given in Figure 4.

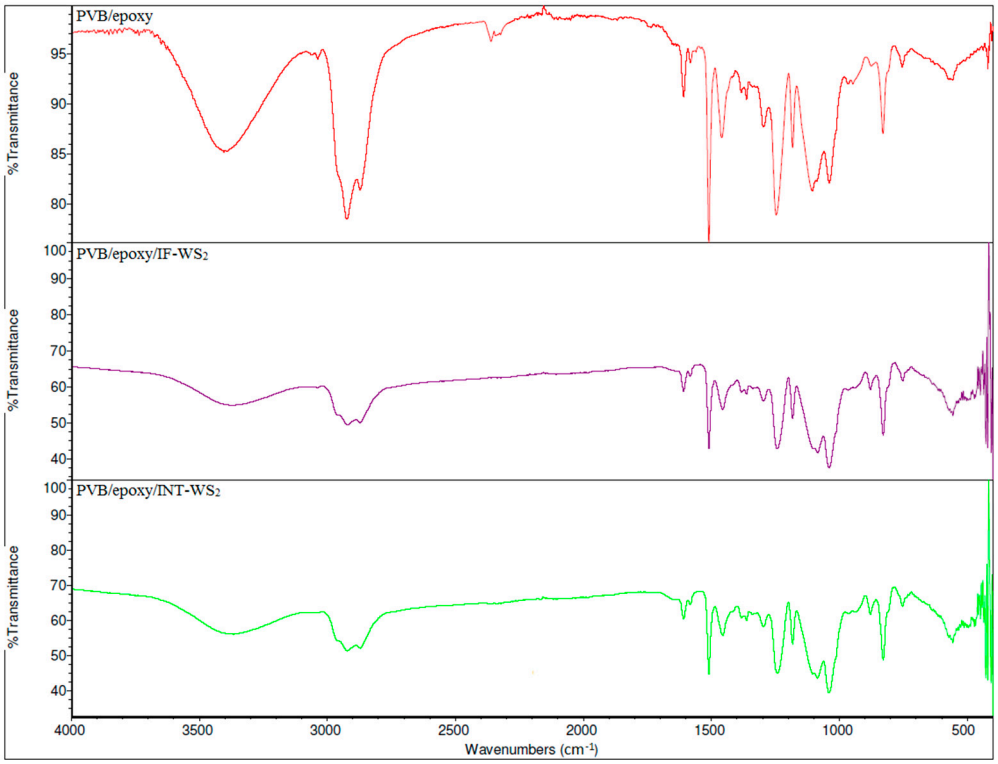


**Figure 4.** FTIR spectra of the prepared coatings.

We may observe the following peaks that are characteristic for PVB in the three FTIR spectra: at 3350–3450 $cm^{-1}$ there is a peak of the -OH group; at 2850 and 3000 $cm^{-1}$ there are peaks for -$CH_3$, -$CH_2$, -CH groups respectively; at 1400 and 1280 $cm^{-1}$ for alkynes; at 1740–1750 $cm^{-1}$ for -C=O; at 1200 $cm^{-1}$ for ester group; at 1100 $cm^{-1}$ for -C-O-C group; and at 950 $cm^{-1}$ for the acetal group. Also, we may observe the peaks that are characteristic for the epoxy resin: at ~920 $cm^{-1}$ vibrations of the epoxy ring; and at the 1670 $cm^{-1}$ the vibrations of the aldehyde groups. Comparing the FTIR curves for the reference sample of the PVB/epoxy polymer blend with those containing $WS_2$ nanostructures, a mild difference in the intensity of the -OH peak can be observed. The intensity of this peak has been somewhat reduced most probably as a consequence of a more complete cross-linking reaction between PVB and epoxy resin in the samples with $WS_2$. The presence of these nanostructures may have caused easier mobility of the polymer molecules so the reactive functional groups could interact in a higher extent, in the inter-phase on the surface of the incorporated nanostructures [41,58,59]. The slight reduction in the intensity of the OH band may be associated with changes in the hydrogen-bonding environment and the curing process. The incorporation of $WS_2$ nanostructures may restrict the mobility of the polymer chains in their surrounding through physical interactions with the matrix. This interpretation is consistent with the observed increase in $T_g$ (Section 3.4) and the improved mechanical properties of the coatings (Section 3.5).

In addition to the observed difference in the intensity of the -OH peak, the FTIR curves are very similar for all the examined samples, indicating that the present $WS_2$ nanostructures are chemically inert. This suggests that their mechanical reinforcing effect

and their influence on the spectrophotometric behavior of the analyzed coatings result from the physical interaction of $WS_2$ nanostructures with the polymer matrix and from their inherent properties. The observed interaction of tungsten disulfide nanotubes and fullerene-like nanoparticles with a polymer matrix based on polyvinyl butyral and epoxy resin may involve several physicochemical and mechanical processes that affect the dispersion, compatibility, and ultimate properties of the composite coatings. A possible explanation of the interaction mechanisms may lie in the physical interactions, like Van der Waals forces. It is known that $WS_2$ nanostructures may exhibit strong Van der Waals forces between their layers and with the surrounding polymer matrix [60], which can improve the adhesion to the PVB/epoxy matrix but may also lead to agglomeration if not properly dispersed. Also, there may be so-called mechanical interlocking: the nanotubes and fullerene-like nanoparticles can become physically embedded in the polymer network, contributing to the coating's reinforcement. Their shape and surface roughness play a role in keeping them in good adhesion with the matrix [60,61]. In addition to physical interactions, weak interfacial interactions, such as hydrogen bonding between the hydroxyl groups of the PVB matrix and the surface of the $WS_2$ nanostructures, may also contribute to the adhesion between the nanofiller and the polymer matrix. Although no evidence of chemical surface functionalization was observed by FTIR, these non-covalent interactions may improve the compatibility and dispersion of the nanostructures within the PVB/epoxy matrix, thereby contributing to the enhanced mechanical performance of the coatings. Also, the formation of the hydrogen bonds between the $WS_2$ nanostructures and hydroxyl groups in PVB can enhance their adhesion to the polymer matrix. Another chemical interaction that certainly takes place in the observed system is the reaction of PVB with epoxy [28], the crosslinking during curing, into a dense crosslinked network. The $WS_2$ nanostructures may interact with this network, either by providing nucleation sites for crosslinking or by being "trapped" within the network. Such interactions of the reinforcement with the polymer matrix might provide improved mechanical properties.

### *3.4. DSC Analysis Results*

The values of $T_g$ for the examined coatings samples are given in Table 1, while the registered DSC thermographs from the cycle heating-cooling-heating are provided in Supplementary Material, in Figures S1–S3.

**Table 1.** Glass transition temperatures of the composite coatings.

| | Samples | $T_g$ (II Heating), °C |
|---|---|---|
| 1. | PVB/epoxy | 82.0 |
| 2. | PVB/epoxy/IF-$WS_2$ | 84.3 |
| 3. | PVB/epoxy/INT-$WS_2$ | 87.3 |

As observed, the addition of IF-$WS_2$ and INT-$WS_2$ to the PVB/epoxy system had a positive effect on the thermal stability/ thermal resistance of the material. Nanotubular form of $WS_2$ provides the increase in $T_g$ for more than 5 °C. The explanation for the increased $T_g$ values may be in the fact that the nanostructures of tungsten disulfide have high thermal resistance themselves, but also that the incorporation of $WS_2$ enhances the thermal conductivity of the matrix, helping the heat dissipation [31,62]. This can be particularly useful in high-temperature or thermally dynamic environments.

### *3.5. Hardness of the Coatings*

The average values of the measured hardness of the analyzed coatings are given in Table 2.

**Table 2.** Hardness of the examined coatings.

| Coating Sample | Shore D Hardness ± st. dev. |
|---|---|
| PVB/epoxy | 83.7 ± 1.6 |
| PVB/epoxy/IF-$WS_2$ | 88.6 ± 1.8 |
| PVB/epoxy/INT-$WS_2$ | 98.2 ± 0.7 |

From the observed results, we may tell that the incorporated reinforcement has provided expected increase in the coating's hardness. The standard deviations were relatively small, so the obtained coatings had uniform hardness property over the surface, due to uniform distribution of previously deagglomerated reinforcements. Aside from the inherent mechanical strength of the reinforcements that is the main cause of the hardness improvement, the interaction between the PVB/epoxy matrix and the nanostructures is responsible for the improvement as well. While improving hardness, $WS_2$ nanotubes can maintain the polymer's flexibility, balancing brittleness and toughness, due to their shape. The incorporation of these nanostructures should also provide enhanced impact resistance [60], where the particulates should absorb and dissipate impact energy, reducing the cracks or fractures in the coating.

### *3.6. Ultrasonic Cavitation Test Results—Resistance to Cavitation Wear*

The cavitation erosion resistance of the tested materials was evaluated based on cumulative mass loss measurements obtained under ultrasonic cavitation. The resulting mass loss of the hybrid coatings samples after each cycle of the ultrasonic cavitation wear test is given in Table 3. The cumulative curves of the mass loss are given in Figure 5, and the appearance of the examined samples is shown in Figure 6.

**Table 3.** Cavitation wear resistance—mass loss.

| Sample/Mass Loss in Time | 15 min | 30 min | 45 min | 60 min | 75 min | Total Mass Loss, mg |
|---|---|---|---|---|---|---|
| | $\Delta m_1$, mg | $\Delta m_2$, mg | $\Delta m_3$, mg | $\Delta m_4$, mg | $\Delta m_5$, mg | |
| PVB/epoxy | 1.4 | 1.1 | 1.6 | 0.9 | 0.8 | 5.8 |
| PVB/epoxy/ IF-$WS_2$ | 1.1 | 0.8 | 1.3 | 0.8 | 0.4 | 4.4 |
| PVB/epoxy/INT-$WS_2$ | 0.7 | 1.0 | 1.2 | 1.1 | 0.5 | 4.5 |

As may be observed, the failure mechanism includes brittle cracks, surface erosion and fissures on the surface of square-shaped composite samples. All the samples submitted to ultrasonic cavitation wear test had similar damage in the middle of the sample's surface, although in the case of the coating PVB/epoxy this is not easy to see due to white color of the sample. However, from Table 3 and Figure 5, it is evident that all the examined samples exhibit gradual mass loss with a similar trend in cavitation curves. As in similar studies [54,55,61–63], in this study it was confirmed that the presence of particulate or a tubular filler of high hardness and wear resistance can improve the overall wear resistance of the polymer matrix into which it was incorporated.

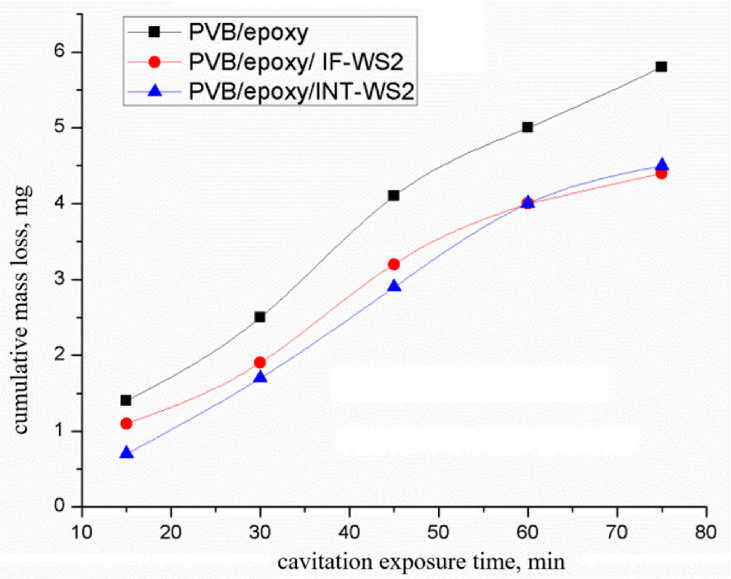


**Figure 5.** Cumulative mass loss curves from the cavitation erosion test.

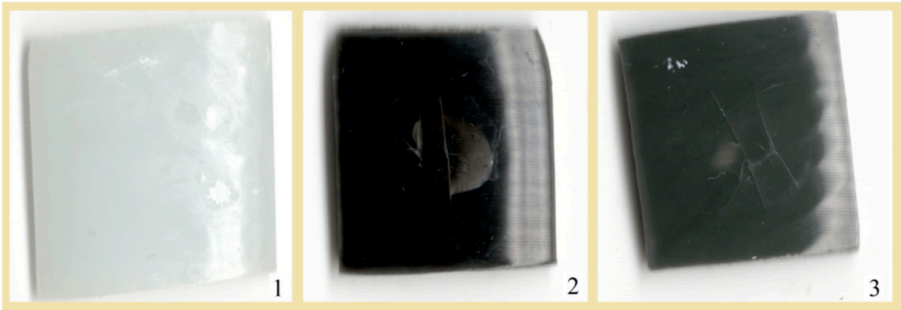


**Figure 6.** Appearance of the composite coating's surface after the cavitation wear test: PVB/epoxy (**1**), PVB/epoxy/ IF-$WS_2$ (**2**), PVB/epoxy/INT-$WS_2$ (**3**).

The reference PVB/epoxy sample exhibited the highest total mass loss (5.8 mg), indicating the lowest resistance to cavitation-induced damage. The incorporation of $WS_2$ nanostructures significantly improved the cavitation resistance, reducing the total mass loss of 4.4 mg and 4.5 mg for IF-$WS_2$ and INT-$WS_2$ reinforced composites, respectively. This corresponds to an improvement of approximately 22%–24% compared to the unmodified matrix. The enhanced performance can be attributed to the ability of $WS_2$ nanostructures to dissipate impact energy, due to their intrinsic mechanical resistance [30–32,60]. In the polymer matrix, these structures can reduce crack initiation and propagation. The IF-$WS_2$-reinforced composite showed slightly better cavitation resistance, which is in accordance with the shape of these particles. As they are close to spherical morphology, we may assume that they may provide a more uniform stress distribution in the matrix in which they are incorporated. Regarding the INT-$WS_2$, they also provide good dissipation of the energy absorbed from the cavitation and contribute to improved cavitation resistance compared to the neat polymer. As can be observed from the listed mass losses, there is a relatively small difference between IF-$WS_2$ and INT-$WS_2$, so we may conclude that both nanofillers are effective in improving cavitation resistance.

### *3.7. Camouflage Behavior of the Coatings—Spectrophotometric Results*

Figure 7 shows the diffuse reflection and transmittance curves for the analyzed coatings in the selected part of the spectrum.

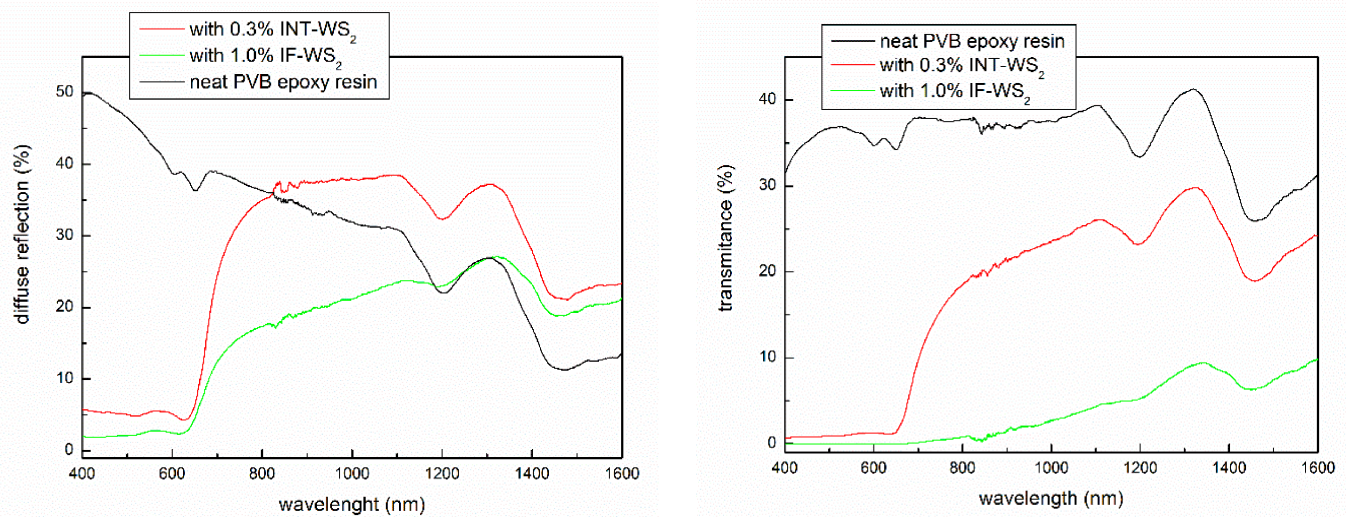


**Figure 7.** Diffuse reflection (**left**) and transmittance (**right**) for the analyzed coatings.

The values for the specular gloss are given in Table 4, for the coatings with and without nanofillers. The results are given as mean values of five measurements.

**Table 4.** Specular gloss for the analyzed coatings.

| Sample | Gloss, GU 20° |
|---|---|
| PVB/epoxy | 89.0 |
| PVB/epoxy/ IF-$WS_2$ | 58.9 |
| PVB/epoxy/ INT-$WS_2$ | 84.5 |

The effects $WS_2$ nanostructures have on the spectrophotometric properties of the PVB/epoxy system, i.e., on the camouflage potential of the coatings thereof, are the consequences of the interactions of nanostructures with light [3,44,48]. There are several potential explanations or the reasons for such behavior of the novel coating materials. These nanostructures may interact with light in such a way to alter the optical properties of the coating due to the fact that their dispersion influence the extent of light scattering and absorption, which is crucial for camouflage or anti-glare applications. The dimensions and morphology of $WS_2$ nanostructures affect how they scatter light. Fullerene-like nanoparticles provide isotropic scattering, since their shape is close to spherical. The nanotubes have high length-to-diameter ratio so they may introduce anisotropic scattering depending on their alignment in the polymer matrix. The addition of $WS_2$ nanostructures disrupts the uniformity of the coating, i.e., introduces heterogeneity in the polymer matrix, affecting how light propagates through the material. The incident light is scattering and reducing the amount of light transmitted through the coating. The nanostructures scatter light in multiple directions, reducing specular gloss and creating a more matte surface, which is beneficial for the camouflage behavior of the material, by reducing glare. Also, the incorporation of $WS_2$ nanostructures changes the refractive index of the coating. A greater difference between the coating and the underlying glass or the surrounding air enhances light scattering. It is important to note that in case of coating systems like this, with dispersed functional nanostructures, even with good dispersion, some degree of aggregation may occur. This may cause surface roughness at the micro- or nano-scale, which contributes to diffuse reflectance and gloss reduction.

The anisotropic shape of $WS_2$ nanotubes can scatter polarized light differently from unpolarized light, which can enhance the camouflage masking, i.e., the stealth capability of

the coating by altering its visibility under polarized light conditions, often used in detection systems [44,46,64]. The obtained results have some similarities, but also some differences compared to findings from previously conducted research [65]. In earlier studies, the nanofillers were not dispersed in epoxy resin, as in this case, but even so these epoxy dispersed samples maintained the desirable spectrophotometric behavior. The difference between spectrophotometric values could be a consequence of epoxy resin dispersion of nanofillers or their above-mentioned agglomeration. Moreover, compared to available data of commercially used glasses [66], it can be seen that nanomodified samples used in this research have transmittance values that are similar to heat-absorbing glasses. This finding marks another possible application of these enhanced materials.

Further research and development of these new hybrid coatings should address several challenges regarding their processing technology, in order to achieve optimal quality. Without proper functionalization or dispersion techniques, $WS_2$ nanostructures may aggregate, and this agglomeration might diminish their effectiveness. A weak interface between $WS_2$ and the matrix may lead to reduced mechanical reinforcement. Functionalization or surfactants can improve interfacial adhesion and bonding. By understanding and optimizing these interactions, $WS_2$ nanostructures can significantly enhance the performance of PVB/epoxy coatings on glass, providing improved mechanical strength, optical properties, and durability for advanced applications. By adjusting the concentration of $WS_2$ nanostructures, the coating's ability to absorb or scatter certain wavelengths can be fine-tuned to match the surrounding environment for better camouflage performance. At lower concentrations, the $WS_2$ nanostructures might enhance light scattering without significantly impacting transparency, maintaining moderate camouflage effects. At higher concentrations, the nanostructures may dominate light absorption and scattering, resulting in enhanced masking and more pronounced camouflage effects, but also in decreased transparency. In further work, long-term environmental durability of the developed coatings will be evaluated, including exposure to humidity, UV radiation, temperature cycling, and weathering conditions, as essential for practical applications of protective coatings. However, these investigations were beyond the scope of the present study, which focused on the initial development and characterization of the $WS_2$-reinforced transparent coatings. Also, in order to cover the multispectral camouflage demands, the future work should infrared thermography examinations, spectral matching analysis between the coated glass and typical military background spectra, and EMS analyses. From the aspect of the mechanical resistance, it would be important to perform adhesion and tribological characterization (pull-off adhesion, cross-cut adhesion, nanoindentation or wear testing) as well as the influence of coating thickness on the observed characteristics.

## 4. Conclusions

New hybrid PVB/epoxy coatings reinforced with functional nanostructures of tungsten disulfide in the form of fullerene-like nanoparticles and nanotubes have been developed and examined. Glass plates coated with the composite coatings were submitted to spectrophotometric examination, and the coatings were thermo-mechanically tested. The coating samples with $WS_2$ showed increased thermal resistance, as higher glass-transition temperatures were obtained ($T_g$ increased by 2.32 °C and 5.32 °C with addition of IF-$WS_2$ and INT-$WS_2$, respectively). These coatings also exhibited greater resistance to cavitation wear (by 22%–24%) and higher hardness (improved from 83.7 to 98.2 Shore D). The addition of tungsten disulfide nanostructures modifies the optical and camouflage properties of PVB/epoxy coatings, resulting in more pronounced camouflage masking compared to the neat material. This modification increases light scattering and absorption, reducing gloss and specular reflectance. Due to the unique mechanical, optical, and chemical

properties of fullerene-like nanoparticles and nanotubes of $WS_2$, PVB/epoxy coatings with these nanostructures on glass can be used as multifunctional materials with applications in defense, architecture, and advanced optics. Further research should encompass adjustments of nanostructure concentrations and potentially rheological behavior of the PVB/epoxy system with the incorporated $WS_2$ in order to achieve scale-up of the application of these coatings, as well as long-term environmental durability of the developed coatings, multispectral camouflage evaluation, adhesion and tribological characterization, and the optimization of coating thickness.

**Supplementary Materials:** The following supporting information can be downloaded at: https://www.mdpi.com/article/10.3390/coatings16070846/s1, Figure S1: DSC thermographs for PVB/epoxy; Figure S2: DSC thermographs for PVB/epoxy/IF-$WS_2$; Figure S3: DSC thermographs for PVB/epoxy/INT-$WS_2$.

**Author Contributions:** Conceptualization, D.M.B. and A.S.; methodology, D.M.B., A.S., A.A. and B.F.; validation, M.P. and A.S.; formal analysis, A.S., B.F. and D.M.B.; investigation, D.M.B., A.S., A.A. and B.F.; resources, D.M.B. and M.P.; data curation, D.M.B., A.A. and A.S.; writing—original draft preparation, D.M.B., A.S. and B.F.; writing—review and editing, D.M.B., A.S., M.P., A.A. and B.F.; visualization, A.S. and D.M.B.; supervision, D.M.B.; project administration, M.P. All authors have read and agreed to the published version of the manuscript.

**Funding:** This research received no external funding.

**Institutional Review Board Statement:** Not applicable.

**Informed Consent Statement:** Not applicable.

**Data Availability Statement:** There were no additional data except those presented in the paper. These data are available per request from the authors.

**Acknowledgments:** This work was supported by the Ministry of science, technological development and innovations (Serbia), Contract No. 451-03-34/2026-03/200325, 451-03-33/2026-03/200017, 451-03-33/2026-03/200036.

**Conflicts of Interest:** The authors declare no conflict of interest.

## References

1. Shirke, N.; Ghase, V.; Jamdar, V. Recent advances in stealth coating. *Polym. Bull.* **2024**, *81*, 9389–9418. [CrossRef]
2. Kostić, I.; Pavlović, D.; Lazović, V.; Vasiljević, D.; Stojanović, D.; Knežević, D.; Tomić, L.; Dikić, G.; Pantelić, D. Thermal and Camouflage Properties of Rosalia alpina Longhorn Beetle with Structural Coloration. In Proceedings of the 7th International Scientific Conference on Defensive Technologies: OTEH 2016, Belgrade, Serbia, 6–7 October 2016; pp. 525–529.
3. Samolov, A.; Pijević, D.; Knežević, D.; Mišković, K.; Sirovatka, R.; Bajić, D. Tunable Spectral Properties of PVB/$WS_2$ Impregnated Fabrics in VIS, IR and RF Part of the EMS. *J. Ind. Text.* **2024**, *54*, 15280837241291613. [CrossRef]
4. Zhang, B.; Xu, C.; Xu, G.; Xiang, S.; Zhu, Y. Thermochromic and infrared emissivity characteristics of cobalt doped zinc oxide for smart stealth in visible-infrared region. *Opt. Mater.* **2018**, *86*, 464–470. [CrossRef]
5. Koch, K.W.; Lin, L.; Price, J.J.; Kim, C.-G.; Moon, D.-G.; Oh, S.-Y.; Oh, J.-K.; Oh, J.-H.; Paulson, C.A.; Zhang, B.; et al. Wavelength-Selective Coatings on Glass with High Hardness and Damage Resistance. *Coatings* **2020**, *10*, 1247. [CrossRef]
6. Demirhan, Y. Anti-reflective and optical transparent coatings fabricated by a computer-controlled system. *Opt. Quant. Electron.* **2026**, *58*, 75. [CrossRef]
7. Anti-Reflective and Anti-Glare Glass. Available online: https://www.corning.com/worldwide/en/innovation/materials-science/surface-impressions.html (accessed on 31 May 2026).
8. Paulson, C.A.; Price, J.J.; Koch, K.W.; Kim, C.-G.; Oh, J.-H.; Lin, L.; Subramanian, A.N.; Zhang, B.; Amin, J.; Mayolet, A.; et al. Industrial-grade anti-reflection coatings with extreme scratch resistance. *Opt. Lett.* **2019**, *44*, 5977–5980. [CrossRef] [PubMed]
9. Price, J.J.; Xu, T.; Zhang, B.; Lin, L.; Koch, K.W.; Null, E.L.; Reiman, K.B.; Paulson, C.A.; Kim, C.-G.; Oh, S.-Y.; et al. Mechanically Tunable Anti-Reflection Coatings. *Coatings* **2021**, *11*, 213. [CrossRef]

10. Sharma, N.; Pal, S.; Kamparath, R.; Subrahmanyam, V.V.V.; Sharma, N.; Mandal, S.K.; Karwal, S.; Gupta, P.; Benerji, N. Low-Refractive Index $Ta_2O_5$ versus Hybrid $TiO_2$–$SiO_2$ for Laser-Durable Broadband Antireflection Coatings. *ACS Appl. Opt. Mater.* **2026**, *4*, 949–961. [CrossRef]
11. Liu, K.; Zhang, S.; He, J. Preparation of Robust, Antireflective and Superhydrophobic Hierarchical Coatings on PMMA Substrates via Mechanical Locking and Chemical Bonding. *ACS Appl. Mater. Interfaces* **2025**, *17*, 4044–4054. [CrossRef] [PubMed]
12. Liu, H.; Lu, Q.; Zhao, Q.; Qiao, C.; Tao, F.; Ji, X.; Liu, L.; Wang, Z. Bioinspired Broadband Omnidirectional Anti-Reflective Coatings by Scalable Dip-Coating Process for Efficient Solar Energy Collection. *Adv. Funct. Mater.* **2026**, *5*, e75998. [CrossRef]
13. Jafari, H.; Mehrizi, K.M.; Fattahi, S. The effect of inorganic nanoparticles on camouflage properties of cotton/polyester fabrics. *Prog. Color Color. Coat.* **2016**, *9*, 29–40. [CrossRef]
14. Arukula, R.; Kim, T.; Lu, S.; Qi, X. Design and characterization of visually opaque but near-infrared transparent coatings for better barcode readability. *Sci. Rep.* 2026, *in press*. [CrossRef] [PubMed]
15. Marković, S.; Stojanović, Z.S.; Veselinović, L.; Simić, D.; Samolov, A.; Stojković Simatović, I. HAp:Co as tunable VIS-NIR reflective pigment. In Proceedings of the 9th International Scientific Conference on Defensive Technologies: OTEH 2020, Belgrade, Serbia, 15–16 October 2020; pp. 475–480. Available online: https://hdl.handle.net/21.15107/rcub_dais_10038 (accessed on 31 May 2026).
16. Kumar, N.; Dixit, A. *Nanotechnology for Defense Applications*; Springer Nature: Cham, Switzerland, 2019. [CrossRef]
17. „We Are Binding" is Our Motto as MOWITAL® Polyvinyl Butyral (PVB) Specialists. Available online: https://www.kuraray.eu/products-solutions/product-groups/polyvinyl-butyral (accessed on 12 June 2026).
18. Yao, H.; Zhang, X.; Shen, L.; Bao, N. Tribological and Anticorrosion Properties of Polyvinyl Butyral (PVB) Coating Reinforced with Phenol Formaldehyde Resin (PF). *Prog. Org. Coat.* **2021**, *158*, 106382. [CrossRef]
19. Ipakchi, H.; Rezadoust, A.M.; Esfandeh, M.; Rezaei, M. An investigation on the effect of polyvinyl butyral interlayer forms on the fracture toughness of glass reinforced phenolic laminates. *Thin-Walled Struct.* **2020**, *151*, 106724. [CrossRef]
20. Ren, J.; Dong, W.; Zhong, Y.; Idrisheva, Z.; Toshtay, K.; Xie, P.; Hou, H. Two Dimensional Graphene and One Dimensional Magnetite@Polyaniline Reinforced Epoxy Nanocomposites with Excellent Electromagnetic Wave Absorption Performance Prepared by Hot Pressing Method. *Eng. Sci.* **2026**, *39*, 1939. [CrossRef]
21. Tochaikul, G.; Tanadchangsaeng, N.; Panaksri, A.; Moonkum, N. Enhancing Radiation Shielding Capabilities with Epoxy-Resin Composites Reinforced with Coral-Derived Calcium Carbonate Fillers. *Polymers* **2025**, *17*, 113. [CrossRef] [PubMed]
22. Çakir, M.; Akin, E.; Renda, G. Mechanical properties of carbon-aramid hybrid fiber-reinforced epoxy/poly(vinyl butyral) composites. *Polym. Compos.* **2023**, *44*, 4826–4841. [CrossRef]
23. Ali, M.F.; Hussain, M.; Tariq, A.; Ahmed, H.I.; Shahid, S.; Saouab, A.; Nawab, Y. Damage-Tolerant Woven Glass Fiber Composites Developed Using Polyvinyl Butyral (PVB) Unsaturated Polyester (UP) Blends. *Adv. Mater. Sci. Eng.* **2022**, *2022*, 9077788. [CrossRef]
24. Nash, N.; Young, T.M.; McGrail, P.T.; Stanley, W.F. Inclusion of a thermoplastic phase to improve impact and post-impact performances of carbon fibre reinforced thermosetting composites—A review. *Mater. Des.* **2015**, *85*, 582–597. [CrossRef]
25. Xiang, H.; Lin, Y.; Fang, G. Thermal Properties of Polyvinyl Butyral/Graphene Composites as Encapsulation Materials for Solar Cells. *Sol. Energy* **2018**, *161*, 187–193. [CrossRef]
26. Zhu, Z.; Zongmin, W.; Chen, S.; Liu, Y.; Zhang, Y.; Wang, W. Enhanced Anticorrosion Properties of Composite Coatings Containing Polyvinyl Butyral and Polyaniline-carbonized Polyaniline. *Prog. Org. Coat.* **2023**, *180*, 107559. [CrossRef]
27. Simić, D.M.; Stojanović, D.B.; Dimić, M.; Totovski, L.; Brzić, S.; Uskoković, P.S.; Aleksić, R.R. Preliminary analysis of the possibility of preparing PVB/IF-$WS_2$ composites. Effect of nanoparticles addition on thermal and rheological behavior of PVB. *Sci. Tech. Rev.* **2016**, *66*, 15–21.
28. Marjanović, M.; Bajić, D.; Perković, S.; Fidanovski, B.; Burzić, Z.; Matija, L. Inorganic fullerene-like nanoparticles and nanotubes of tungsten disulfide as reinforcement of carbon-epoxy composites. *Fuller. Nanotub. Carbon Nanostruct.* **2021**, *29*, 1034–1044. [CrossRef]
29. Sethulekshmi, A.S.; Jayan, J.S.; Saritha, A.; Joseph, K. Insights into the reinforcibility and multifarious role of $WS_2$ in polymer matrix. *J. Alloys Compd.* **2021**, *876*, 160107. [CrossRef]
30. Tenne, R. Recent advances in the research of inorganic nanotubes and fullerene-like nanoparticles. *Front. Phys.* **2014**, *9*, 370–377. [CrossRef]
31. Tenne, R. Inorganic nanotubes and fullerene-like materials of metal dichalcogenide and related layered compounds. In *Nanomaterials Handbook*; Gogotsi, Y., Ed.; CRC Press Taylor & Francis Group: Boca Raton, FL, USA; London, UK; New York, NY, USA, 2006; pp. 317–338. [CrossRef]
32. Tenne, R. Inorganic nanotubes and fullerene-like nanoparticles. *Nat. Nanotech.* **2006**, *1*, 103–111. [CrossRef] [PubMed]
33. Ghosh, S.; Otorgust, G.; Idelevich, A.; Regev, O.; Lapsker, I.; Lewitus, D.Y.; Zak, A. Reinforcement of poly (methyl methacrylate) by $WS_2$ nanotubes towards antiballistic applications. *Compos. Sci. Technol.* **2021**, *207*, 108736. [CrossRef]
34. Stojanović, D.B.; Obradović, V.; Bajić, D.; Uskoković, S. A new generation of aramid fibers/poly (vinyl butyral) composites for ballistic protection: Recent development and advances. *J. Eng. Fibers Fabr.* **2024**, *19*, 15589250241309084. [CrossRef]

35. Zohar, E.; Baruch, S.; Shneider, M.; Dodiuk, H.; Kenig, S.; Wagner, D.; Zak, A.; Moshkovith, A.; Repoport, L.; Tenne, R. The mechanical and tribological properties of epoxy nanocomposites with $WS_2$ nanotubes. *Sens. Transducers* **2011**, *12*, 53–65.
36. Xu, F. Large Scale Manufacturing of IF-$WS_2$ Nanomaterials and Their Application in Polymer Nanocomposites. Ph.D. Thesis, University of Exeter, Devon, UK, 2013.
37. Kaplan-Ashiri, I.; Tenne, R. On the Mechanical Properties of $WS_2$ and $MoS_2$ Nanotubes and Fullerene-Like Nanoparticles: In Situ Electron Microscopy Measurements. *JOM* **2016**, *68*, 151–167. [CrossRef]
38. Wu, S.; Bhat, G.S. Inorganic Fullerene-like Tungsten Disulfide/Waterborne Polyurethane Reinforced Spectra® Composites with Improved Mechanical Properties and Tensile Energy Absorption. *Results Mater.* **2023**, *18*, 100389. [CrossRef]
39. Orikasa, K.; Nisar, A.; Dey, P.; Benedetti, L.; Dolmetsch, T.; Thomas, T.; Agarwal, A. Exploring thermal and in-situ mechanical properties of flexible 2D tungsten disulfide foam-polymer composite for thermal management. *Compos. Part B Eng.* **2024**, *284*, 111743. [CrossRef]
40. Cheng, X.; Zhang, W.; Wang, C.; Chen, S.; Tang, Z.; Zhang, L. 2D WS2/Polyimide Composite Films With Enhanced Mechanical Properties, Electrical Breakdown Strength, and Thermal Stability via Optimized Filler–Polymer Interfaces. *J. Appl. Polym. Sci.* **2026**, *143*, e57917. [CrossRef]
41. Sahu, M.; Narashimhan, L.; Prakash, O.; Raichur, A.M. Noncovalently Functionalized Tungsten Disulfide Nanosheets for Enhanced Mechanical and Thermal Properties of Epoxy Nanocomposites. *ACS Appl. Mater. Interfaces* **2017**, *9*, 14347–14357. [CrossRef] [PubMed]
42. Chen, D.; Cao, X.; Tiwari, S.K.; Ola, O.; Wang, N.; Zhu, Y. Mechanical and thermal degradation behavior of inorganic fullerene-liked tungsten disulfide reinforced perfluoroalkoxy/poly(ether-ether-ketone) nanocomposites. *Polym. Degrad. Stab.* **2022**, *203*, 110041. [CrossRef]
43. Wu, F.; Xia, Y.; Sun, M.; Xie, A. Two-dimensional (2D) few-layers $WS_2$ nanosheets: An ideal nanomaterials with tunable electromagnetic absorption performance. *Appl. Phys. Lett.* **2018**, *113*, 052906. [CrossRef]
44. Gultom, P.; Chiang, J.-Y.; Huang, T.-T.; Lee, J.-C.; Su, S.-H.; Huang, J.-C.A. Structural and Optical Properties of Tungsten Disulfide Nanoscale Films Grown by Sulfurization from W and $WO_3$. *Nanomaterials* **2023**, *13*, 1276. [CrossRef] [PubMed]
45. Kumar, R.; Sahoo, S.; Joanni, E. Composites based on layered materials for absorption of microwaves and electromagnetic shielding. *Carbon* **2023**, *211*, 118072. [CrossRef]
46. Zhang, S.; Hao, Y.; Gao, F.; Wu, X.; Hao, S.; Qiu, M.; Zheng, X.; Wei, Y.; Hao, G. Controllable growth of wafer-scale two-dimensional $WS_2$ with outstanding optoelectronic properties. *2D Mater.* **2024**, *11*, 015007. [CrossRef]
47. Cheng, J.; Jin, Y.; Zhao, J.; Jing, Q.; Gu, B.; Wei, J.; Yi, S.; Li, M.; Nie, W.; Qin, Q.; et al. From VIB- to VB-Group Transition Metal Disulfides: Structure Engineering Modulation for Superior Electromagnetic Wave Absorption. *Nano-Micro Lett.* **2024**, *16*, 29. [CrossRef] [PubMed]
48. Samolov, A.D.; Simić, D.M.; Fidanovski, B.Z.; Obradović, V.M.; Tomić, L.D.; Knežević, D.M. Improvement of VIS and IR camouflage properties by impregnating cotton fabric with PVB/IF-$WS_2$. *Def. Technol.* **2021**, *17*, 2050–2056. [CrossRef]
49. Simić, D.; Stojanović, D.B.; Kojović, A.; Dimić, M.; Totovski, L.; Uskoković, P.S.; Aleksić, R. Inorganic fullerene-like IF-$WS_2$/PVB nanocomposites of improved thermo-mechanical and tribological properties. *Mater. Chem. Phys.* **2016**, *184*, 335–344. [CrossRef]
50. Lazić, D.S.; Simić, D.M.; Samolov, A.D.; Jovanović, D. Properties of standard polymeric and water-based coatings for military camouflage protection with addition of inorganic fulerene-like tungsten disulphide (IF-$WS_2$) nanoparticles. *Sci. Tech. Rev.* **2017**, *67*, 38–44. [CrossRef]
51. Saxena, P.; Shukla, P.; Gaur, M. Thermal analysis of polymer blends and double layer by DSC. *Polym. Polym. Compos.* **2021**, *29*, 11–18. [CrossRef]
52. *ASTM G32-16*; Standard Test Method for Cavitation Erosion Using Vibratory Apparatus. ASTM International: West Conshohocken, PA, USA, 2016. Available online: www.astm.org (accessed on 31 May 2026).
53. Kats, I.M. Investigation of the cavitation resistance of elastic polymer coatings. *Hydrotech. Constr.* **1974**, *8*, 539–544. [CrossRef]
54. Stechishin, M.S.; Martinyuk, A.V.; Bilik, Y.M. Cavitation and Erosion Resistance of Polymeric Materials. *J. Frict. Wear* **2018**, *39*, 491–499. [CrossRef]
55. Taillon, G.; Saito, S.; Miyagawa, K.; Kawakita, C. Cavitation erosion resistance of high-strength fiber reinforced composite material. *IOP Conf. Ser. Earth Environ. Sci.* **2019**, *240*, 062056. [CrossRef]
56. *ASTM E903-12*; Standard Test Method for Solar Absorptance, Reflectance, and Transmittance of Materials Using Integrating Spheres. ASTM International: West Conshohocken, PA, USA, 2020.
57. *SRPS 2813:2006*; Paints and Varnishes—Determination of Specular Gloss of Non-Metallic Paint Films at 20°, 60° and 85° (ISO 2813:1994, including Technical Corrigendum 1:1997). Institute for standardization of Serbia: Belgrade, Serbia, 2006.
58. Tastanova, L.; Bekeshev, A.; Nurlybay, S.; Shcherbakov, A.; Mostovoy, A. Environmentally Sustainable Functionalized $WS_2$ Nanoparticles as Curing Promoters and Interface Modifiers in Epoxy Nanocomposites. *Nanomaterials* **2025**, *15*, 1145. [CrossRef] [PubMed]

59. Maalihan, R.D.; Domalanta, M.R.B.; Corrales, A.C.C.; Caldona, E.B. Advances in interfacially engineered surface-functionalized fillers for multifunctional polymer composite coatings. *Polym. Compos.* **2025**, *46*, 5857–5881. [CrossRef]
60. Simić, D.M.; Stojanović, D.B.; Dimić, M.; Mišković, K.; Marjanović, M.; Burzić, Z.; Uskoković, P.S.; Zak, A.; Tenne, R. Impact resistant hybrid composites reinforced with inorganic nanoparticles and nanotubes of $WS_2$. *Compos. Part B Eng.* **2019**, *176*, 107222. [CrossRef]
61. Pavlović, M.; Cvetković, A.; Dojčinović, M.; Trumbulović, L.; Milovanović, A. Cavitation resistance of basalt-based protective coatings and epoxy system. *Struct. Integr. Life* **2021**, *21*, 185–189.
62. Obradović, V.; Vuksanović, M.; Tomić, N.; Stojanović, D.; Husović, T.V.; Uskoković, P. Improvement in cavitation resistance of poly (vinyl butyral) composite films with silica nanoparticles: A technical note. *Polym. Polym. Compos.* **2021**, *29*, 1664–1669. [CrossRef]
63. Deplancke, T.; Lame, O.; Cavaille, J.Y.; Fivel, M.; Riondet, M.; Franc, J.P. Outstanding cavitation erosion resistance of ultra high molecular weight polyethylene (UHMWPE) coatings. *Wear* **2015**, *328*, 301–329. [CrossRef]
64. Ranjan, P.; Shankar, S.; Popovitz-Biro, R.; Cohen, S.R.; Kaplan-Ashiri, I.; Dadosh, T.; Shimon, L.J.W.; Višić, B.; Tenne, R.; Lahav, M.; et al. Decoration of Inorganic Nanostructures by Metallic Nanoparticles to Induce Fluorescence, Enhance Solubility, and Tune Band Gap. *J. Phys. Chem. C* **2018**, *122*, 6748–6759. [CrossRef]
65. Samolov, A.; Simić, D.; Totovski, L. Spectrophotometric properties of PVB/$WS_2$ thin films. In Proceedings of the 8th International Scientific Conference on Defensive Technologies OTEH 2018, Belgrade, Serbia, 11–12 October 2018; pp. 416–420.
66. Measurement of Solar Transmittance through Plate Glass. Available online: https://www.shimadzu.eu/industries/engineering-materials/measurement-of-solar-transmit2/index.html (accessed on 12 June 2026).